Adsorption (2013) 19:201–208
DOI 10.1007/s10450-012-9441-z

Diffusion of *n*-alkanes in mesoporous 5A zeolites by ZLC method

Zhiping Liu · Weiming Fan · Zhaoteng Xue · Jinghong Ma · Ruifeng Li

Received: 23 May 2012 / Accepted: 26 October 2012 / Published online: 8 November 2012

Abstract Diffusion properties of mesostructured zeolite 5A were investigated by employing *n*-alkanes as probe molecules using the zero length column (ZLC) method. The mesopores were found to enhance molecule diffusion. Moreover, the effective diffusion time constant (D_{eff}/R^2) increased with mesoporosity in the zeolites between 308 K and 393 K, whereas the activation energy decreased with increasing mesopore volume. The effective diffusivity values of *n*-alkanes in mesoporous zeolite 5A were generally higher than that the microporous zeolite 5A sample. This clearly implied the important role of the mesopore in zeolites crystals in facilitating the transport of reaction molecules due to shorter average diffusion path length and less steric hindrance.

Keywords Mesoporous zeolite · 5A zeolite · ZLC method · Diffusion · Activation energy

Electronic supplementary material The online version of this article (doi:10.1007/s10450-012-9441-z) contains supplementary material, which is available to authorized users.

Z. Liu · R. Li (✉)
College of Chemistry and Chemical Engineering, Taiyuan University of Technology, Taiyuan, 030024, China
e-mail: ruifeng_li@hotmail.com

W. Fan · Z. Xue · J. Ma · R. Li
Institute of Special Chemicals, Taiyuan University of Technology, Taiyuan, 030024, China

J. Ma
e-mail: jhma0607@hotmail.com

1 Introduction

Zeolite is a microporous crystalline material with ordered pore structures which are composed of channels or cages with diameters ranging from 0.3 to 1.2 nm. Many remarkable features of zeolites such as narrow pore size distribution (or shape selectivity), high surface area, as well as high thermal and hydrothermal stability, render its wide applications in heterogeneous catalysis and in the separation and purification of gases. In most applications, molecular diffusion plays an important role. The intracrystalline diffusivity of molecular species involved in these processes is often the rate limiting factor in the overall kinetics of the processes (Gunadi and Brandani 2006). In many cases, the adsorption or reaction rate is limited by the low effective diffusivity in zeolite crystals, which is as a result of the size similarity of the target molecules and the micropore diameter of zeolites (Huang et al. 2006; Zheng et al. 2010). Diffusion limitation can be minimized by reducing intracrystalline diffusion path length or creating mesopores in zeolite crystals. Diffusion capability of large molecules in zeolite channels has thereby been improved (Groen et al. 2006; Zhao et al. 2008).

Mesostructured zeolite materials have recently attracted much attention because they have the advantages of both mesoporous and microporous zeolites. However, there are only a few articles discussing the kinetics and the diffusion of hydrocarbons in mesoporous zeolite materials (Gobin et al. 2007; Newalkar et al. 2001, 2003; Thang et al. 2003).

Recently, our research group has reported a mesoporous structured zeolite 5A with an intracrystalline nano-cage successfully synthesized using organic functionalized fumed silica as the silica source. The mesoporous zeolite 5A has nano-cages of 3 nm interconnected with each other through 0.8–1.2 nm channels (Xue et al. 2012). Using the zero-length column (ZLC) method, this paper further investigates

the diffusion properties of mesostructured zeolite 5A with probe molecules *n*-alkanes. The promotion effects of intracrystalline mesopore on molecule diffusion in the zeolites are also evaluated.

2 Experimental

2.1 Preparation and characterization of samples

Zeolite 5A with intracrystalline mesopores was prepared according to a synthetic method reported by our research group. Before the synthesis, fumed silica was functionalized with phenylaminopropyl–trimethoxysilane (Y-5669). Then zeolite 4A with intracrystalline mesopores was prepared with the organic functionalized fumed silica as the silica source at a molar composition of Na_2O:Al_2O_3:SiO_2:H_2O = 5:1:1:185. More detailed account of the procedure was provided elsewhere (Xue et al. 2012). By varying the degree of silanization of the silica surface, two mesoporous zeolite 4A samples and corresponding Ca-exchanged mesoporous zeolite 5A with different mesoporosity were obtained and denoted as 5A-1 and 5A-2. The microporous zeolite 5A-0 as a reference sample was synthesized following the same procedure except that the silica source was the unfunctionalized silica.

N_2 adsorption/desorption isotherms of samples at 77 K were obtained on a Quantachrome NOVA 1200e. Field emission scanning electron microscope (Fe-SEM) images were recorded on a JEOL JSM-6700F.

2.2 Adsorption isotherms measurements

The adsorption isotherms of the representative probe adsorbate *n*-octane on three samples were measured by a high-precision intelligent gravimetric analyzer (IGA-002, Hiden) for verification of the linear region used in the ZLC measurements. Before the measurement, the zeolite sample was outgassed at 723 K under vacuum below 10^{-7} mbar until a constant sample weight. During the measurement, a small dose of high purity *n*-octane vapor enough to keep the adsorption process isothermal was introduced directly to the sample chamber. After reaching a stable equilibrium pressure, the weight change was recorded. Further measurements were made by increasing the vapor pressure in steps.

2.3 ZLC experiments and mathematical modeling

ZLC experimental set-up is shown in Fig. 1. ZLC column was packed with 1–2 mg of the zeolite sample, placed between two porous sintered discs in a 1/8 in Swagelok union and located inside a gas chromatograph oven (Agilent 1790). The adsorbate concentration at the ZLC column was adjusted and maintained at a low level enough (0–0.05 mbar absolute pressure range) to ensure that the measurements were carried out within the linear region of the adsorption isotherm (Henry's law region) as required by the ZLC theory. The desorption part of the measurements was performed by purging with pure helium (99.99 %) at a flow rate high enough to maintain a very low adsorbate concentration at the adsorbent surfaces. This ensured good heat transfer and a desorption process that was controlled by intra-particle diffusion rather than external mass transfer (Hoang et al. 2005; Jiang et al. 2001; Lima et al. 2008; Qiao and Bhatia 2005). The change of effluent adsorbate concentration from the ZLC column was determined by a flame ionization detector (FID), which was connected to a computer for data acquisition and analysis.

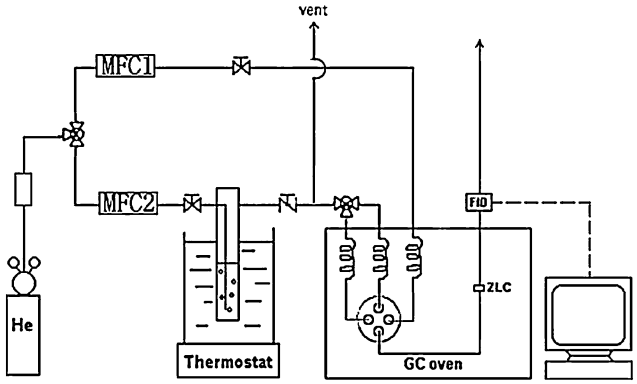

Fig. 1 Schematic diagram of ZLC experiment device

ZLC chromatographic technique was proposed by Eic and Ruthven (1988a) to measure intracrystalline diffusivities in microporous materials. At present, the application of this method has been extended to other systems including biporous materials with both micro- and mesoporosity (Cavalcante et al. 2003; Hufton and Ruthven 1993; Qiao and Bhatia 2005; Stefano 1996).

For a linear equilibrium system with uniform spherical particles and negligible gas hold-up in the voids of the ZLC bed, assuming perfect mixing throughout the ZLC cell, the relative effluent gas concentration (c/c_0) is given by the following equations:

$$\frac{c}{c_0} = 2L \sum_{n=1}^{\infty} \frac{\exp(-\frac{\beta_n^2 D_{\text{eff}} t}{R^2})}{[\beta_n^2 + L(L-1)]} \tag{1}$$

where β_n is given by the roots of the auxiliary equation

$$\beta_n \cot \beta_n + L - 1 = 0 \tag{2}$$

and

$$L = \frac{1}{3} \frac{F}{K V_s} \frac{R^2}{D_{\text{eff}}} \tag{3}$$

in which F is the interstitial gas velocity, R is individual particle radius, Vs is the volume of the solid bed, and K is the dimensionless Henry's Law constant.

Table 1 The pore structural parameters of the different 5A zeolites

Samples	S_{BET} (m^2/g)[a]	S_{mic} (m^2/g)[b]	S_{ext} (m^2/g)[b]	V_{mic} (ml/g)[b]	V_{meso} (ml/g)[c]
5A-0	510	481	29	0.18	0.02
5A-1	501	224	276	0.12	0.08
5A-2	519	149	370	0.09	0.18

[a]BET surface area obtained from N_2 adsorption isotherm in the relative pressure range of 0.05–0.30

[b]Micropore volume was calculated from the *t*-plot method

[c]Mesopore volume was calculated from the BJH method

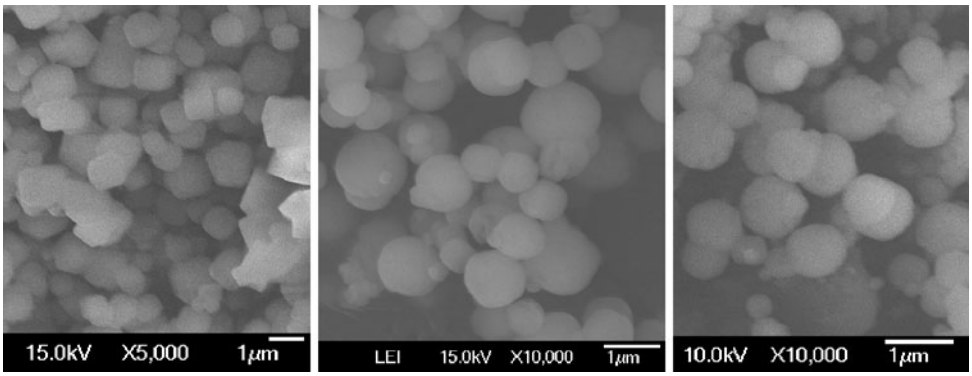

Fig. 2 SEM images of zeolites 5A-0, 5A-1 and 5A-3 (from *left* to *right*)

Effective diffusion time constant (D_{eff}/R^2) could be extracted by fitting Eqs. (1)–(3) with the experimental ZLC data using matlab software tool in the complete time range (Hoang et al. 2005; Stefano 1996; Thang et al. 2003). The effective activation energies were calculated from Arrhenius plots of the corresponding effective diffusivities measured at different temperatures.

3 Results and discussion

The pore structural parameters of microporous zeolite 5A-0, mesoporous zeolite 5A-1 and 5A-2 samples calculated from N_2 adsorption/desorption isotherms are listed in Table 1 and their corresponding SEM images shown in Fig. 2. It is clear from SEM micrographs that microporous zeolite 5A-0 has a typical single-crystal morphology and the crystals are in cubic shapes with truncated edges, while both mesoporous zeolites 5A-1 and 5A-2 are round in shape with rugged surfaces. However, the distributions of the crystals for three samples are similar and the particle diameters fall in the range of 700 to 1000 nm. Moreover, the mesoporous 5A zeolites have greater external surface and mesoporous volume than the microporous zeolite 5A under the same total surface area (S_{BET}), reflecting the coexistence of micropore and mesopore in the mesoporous zeolite 5A-1 and 5A-2 samples. Owing to the similar crystalline particle sizes of the three samples, it is reasonably assessed that the mesopores have existed in the interior of the zeolite crystals. The synthesis and characterization of the zeolite 5A with intracrystalline mesopores was in detail reported in the literature (Xue et al. 2012).

The adsorption equilibrium isotherms of *n*-octane on the different zeolite 5A samples at various temperatures are shown in Fig. 3. At three temperatures, zeolite 5A-0 displays a typical type-I isotherm with the characteristic sharp increase of the isotherm curve at low pressures (<0.1 mbar) corresponding to micropore filling, followed a plateau region at relatively high pressure. The adsorption isotherms of zeolites 5A-1 and 5A-2 show a similar shape to that of zeolite 5A-0 at low pressure region (<0.1 mbar). The adsorption capacities increase sharply with increasing pressure, the extent of which goes in order of 5A-2 < 5A-1 < 5A-0. At relatively high pressure, the adsorption capacities increase progressively with increasing pressure but without the plateau region. The increasing trends are more pronounced on 5A-2 than on 5A-1. Both above observations and results from N_2 adsorption/desorption isotherm data can confirm the microporous and mesoporous characteristics of zeolite 5A-1 and 5A-2.

Figure 4 shows the representative plots of ZLC desorption curves of *n*-octane on zeolite 5A-2 at 308 and 318 K at flow rates of 50 ml/min and 80 ml/min respectively. The partial pressure of *n*-octane was maintained at 0.04 mbar in order to ensure a dilute system (Gunadi and Brandani 2006). The two desorption curves at the same temperature have similar long time slopes, ensuring that the system is controlled by kinetics. In addition, adsorption isotherms of *n*-

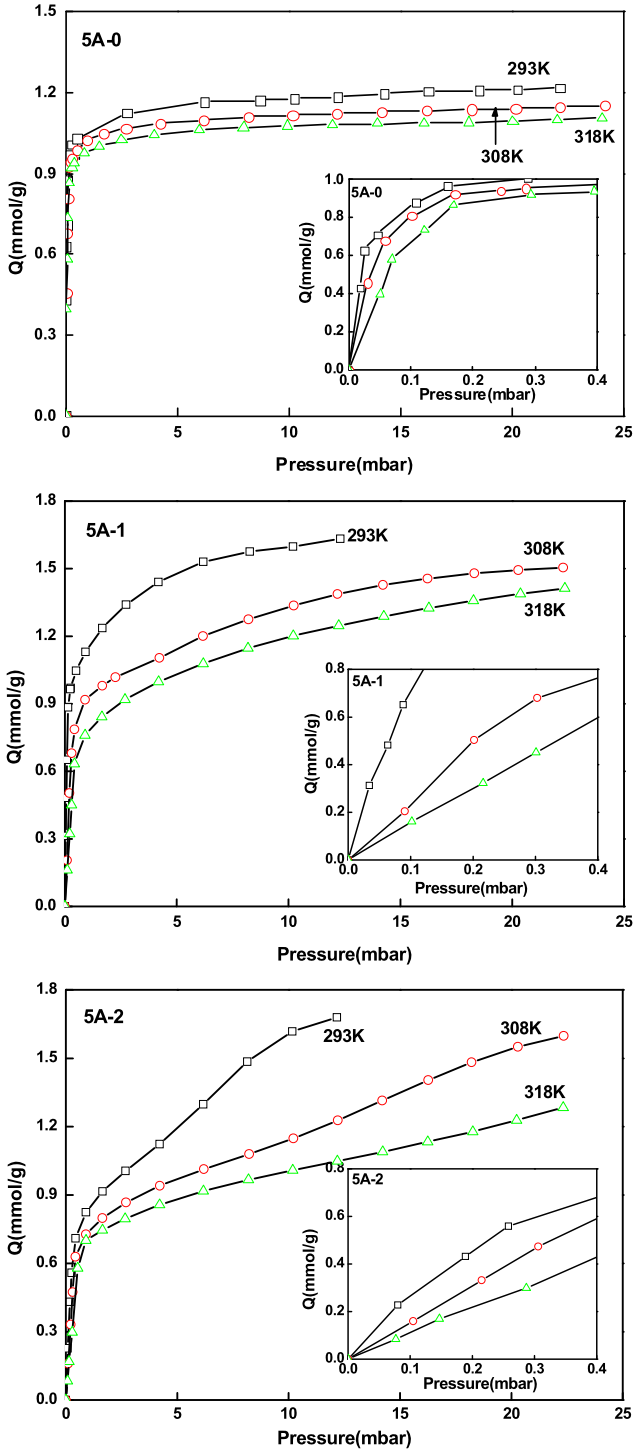

Fig. 3 Adsorption isotherms of *n*-octane on different 5A samples at various temperatures

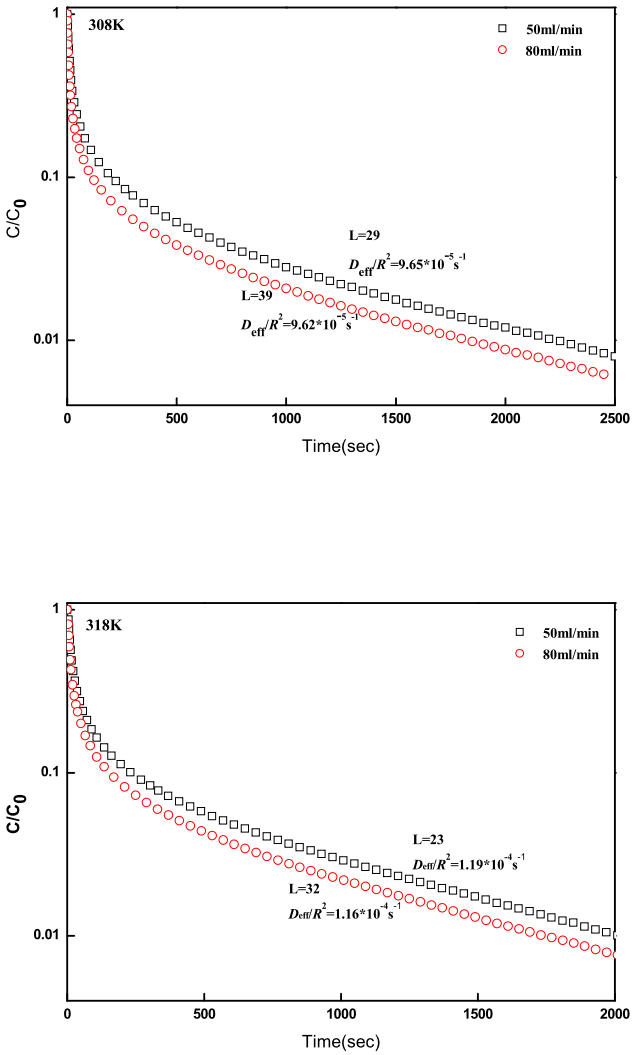

Fig. 4 Desorption curves for *n*-octane on 5A-2 sample at 308 K and 318 K at different flow rates

octane on the three samples at different temperatures (Fig. 3) confirm that the ZLC experiments were conducted in the linear region of the isotherms. i.e. At a low level enough absolute pressure range (0–0.05 mbar), the isotherms for the samples have good linearity (insets in Fig. 3). Only for the 5A-0 sample, at a lower temperature of 298 K, the linearity is poorer than these at higher temperature for the samples possibly because of microporous structure of zeolite 5A without mesopores. However, at 308 and 318 K, the linearity for the three samples is not much doubt. Table 2 shows a summary of diffusion parameters extracted from model fitting of the experimental desorption curves for the three samples at different temperatures and different purge flow rates. At the same temperature, all L values obtained from the theoretical fittings are significantly higher than 10, while F/L and KVs values keep nearly constant. The dimensionless Henry's law constant K decreases with the increase of mesoporosity of 5A, indicating the adsorption weakening of adsorbates on the zeolite surface. The diffusion time constant, D_{eff}/R^2, is essentially independent of the purge flow rate, although the desorption curves are sensitive to purge flow rate. This has also shown that diffusion is kinetically controlled and diffusivities should be

Table 2 Variation of parameters with temperature and purge flow rate for *n*-octane on different 5A samples

T (K)	F (cm^3/min)	L	F/L (cm^3/min)		$D_{eff}/R^2 \times 10^4$ (s^{-1})		$D_{eff} \times 10^{18}$ (m^2/s)	KVs (cm^3)	$K \times 10^{-5}$
			Individual	Average	Individual	Average			
					5A-0				
308	50	38.8	1.29	1.26	0.42	0.42	6.72	166.7	77
	70	57.7	1.21		0.42				
	80	62.6	1.28		0.43				
318	50	30.5	1.64	1.66	0.68	0.68	10.9	135.6	22
	70	42.3	1.65		0.68				
	80	47.2	1.69		0.69				
333	50	25.3	1.98	2.01	0.90	0.91	14.6	122.7	5.6
	70	35.0	2.00		0.90				
	80	39.0	2.05		0.92				
					5A-1				
308	50	21.3	2.35	2.38	0.72	0.72	11.5	183.6	11
	70	28.7	2.44		0.73				
	80	34.0	2.35		0.71				
318	50	27.8	1.80	1.84	0.88	0.88	14.1	116.2	3.7
	70	37.4	1.87		0.87				
	80	43.3	1.85		0.88				
333	50	27.7	1.81	1.83	1.08	1.08	17.3	94.1	1.2
	70	37.5	1.87		1.08				
	80	44.2	1.81		1.08				
					5A-2				
308	50	19.1	2.62	2.59	0.98	0.98	15.7	146.8	2.8
	70	27.8	2.52		0.98				
	80	30.5	2.62		0.98				
318	50	22.3	2.24	2.31	1.09	1.11	17.7	115.6	1.4
	70	30.3	2.31		1.11				
	80	33.5	2.39		1.12				
333	50	19.8	2.53	2.48	1.37	1.35	21.6	102.1	0.5
	70	28.7	2.44		1.34				
	80	32.3	2.48		1.34				

Table 3 Diffusivity Data of *n*-alkanes for different samples at different temperatures

Samples	308 K		333 K		393 K		E_a, kJ/mol
	L	D_{eff}/R^2, s^{-1}	L	D_{eff}/R^2, s^{-1}	L	D_{eff}/R^2, s^{-1}	
				n-Heptane			
5A-0	88.8	0.65×10^{-4}	94.4	0.93×10^{-4}	69.5	2.08×10^{-4}	13.7
5A-1	69.0	1.03×10^{-4}	85.7	1.66×10^{-4}	45.0	2.94×10^{-4}	11.1
5A-2	63.1	1.25×10^{-4}	71.1	1.72×10^{-4}	63.4	3.21×10^{-4}	10.7
				n-Octane			
5A-0	57.7	0.42×10^{-4}	35.4	0.90×10^{-4}	15.0	1.80×10^{-4}	14.8
5A-1	28.7	0.73×10^{-4}	37.6	1.08×10^{-4}	22.3	2.00×10^{-4}	11.8
5A-2	28.1	0.98×10^{-4}	28.7	1.34×10^{-4}	22.4	2.41×10^{-4}	10.8
				n-Decane			
5A-0			54.9	0.63×10^{-4}	97.0	1.48×10^{-4}	15.6
5A-1			51.5	0.80×10^{-4}	106.7	1.56×10^{-4}	12.1
5A-2			66.3	1.09×10^{-4}	56.2	2.00×10^{-4}	11.1

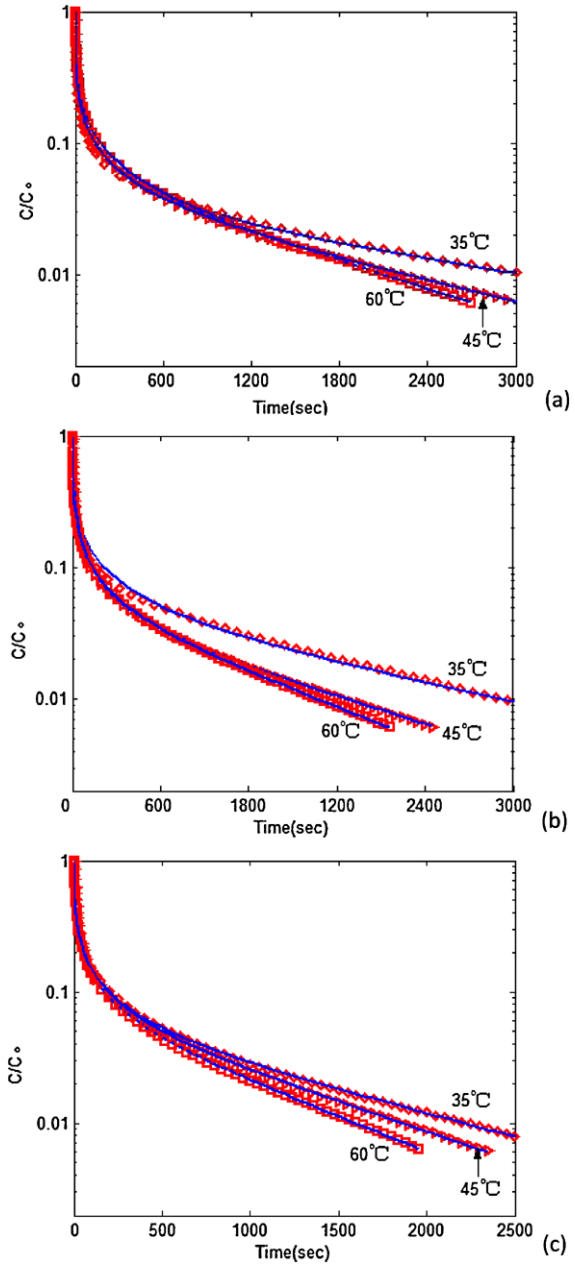

Fig. 5 Experimental (*symbols*) and theoretical (*solid lines*) ZLC curves for *n*-octane at the purge flow rate 70 ml/min and different temperatures: (**a**) 5A-0, (**b**) 5A-1 and (**c**) 5A-2

the same at a given temperature (Qiao and Bhatia 2005; Gunadi and Brandani 2006).

The representative ZLC desorption curves of *n*-octane in 5A zeolites with different mesoporosities at different temperatures are fitted by the ZLC model as shown in Fig. 5. The extracted effective diffusion time constants and corresponding L values of *n*-alkanes series (C_7, C_8, and C_{10}) are listed in Table 3. All L values obtained from the theoretical fittings are greater than 10, indicating that desorption is kinetically controlled as required by the ZLC theory

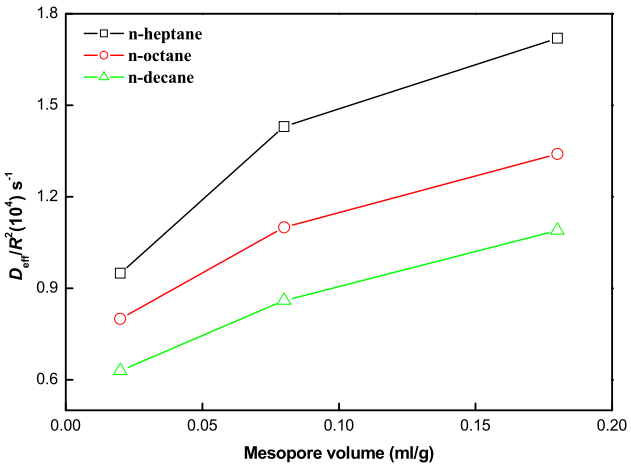

Fig. 6 Effects mesoporous volume of zeolites on effective diffusion time constant at 333 K

(Hoang et al. 2005). A good agreement between the experimental (symbols) and theoretical (solid lines) curves confirms the accuracy of the diffusion time constant extracted from the experiments. As shown in Table 2 and Table 3, the effective diffusion time constant (D_{eff}/R^2) of *n*-alkane in zeolite 5A are consistent with the diffusivities reported previously (Eic and Ruthven 1988b; Gunadi and Brandani 2006). The effective diffusion time constant (D_{eff}/R^2) of *n*-alkanes in zeolite 5A samples in the measured range of 308–393 K confirms the qualitative assessments previously made for the desorption curves. These values increase with mesoporosity in zeolites at each temperature. The effective diffusion time constant (D_{eff}/R^2) of linear alkanes in the mesoporous zeolite 5A is generally found to be higher than that of the reference zeolite 5A sample, indicating an enhanced mass transfer process as a result of the mesoporous structure of the zeolite 5A samples (Fig. 6). Figure 6 also shows that the diffusivity decreases monotonically with increasing chain length from *n*-C_7 to *n*-C_{10}. The variation of diffusivity with the carbon number of *n*-alkanes at different temperature follows a consistent pattern. The effective diffusivity D_{eff} was calculated and listed in Table 2. Obviously, The D_{eff} increases with mesoporosity of 5A. This result is in reasonably good agreement with the earlier report (Gunadi and Brandani 2006). The strong relationship between micro-/meso-structures and diffusivity in the zeolites 5A could be confirmed by the above results. The mesopore structure appears to have strong influence on facilitating the overall transport rate. The limiting step in the diffusion process is dominated by mesopore diffusion influenced by the adsorbate-adsorbent interactions (Lima et al. 2008).

From the measurements at different temperatures, the activation energy (E_a) may be estimated according to the Arrhenius equation. Figure 7 illustrates the dependence of the activation energy of diffusion for linear alkanes on mesopore volume. Effective activation energies of linear alkanes

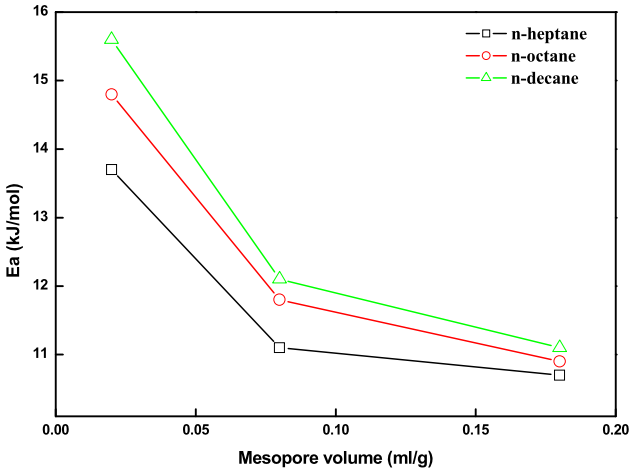

Fig. 7 Change of the activation energy E_a with mesoporous volume of zeolites

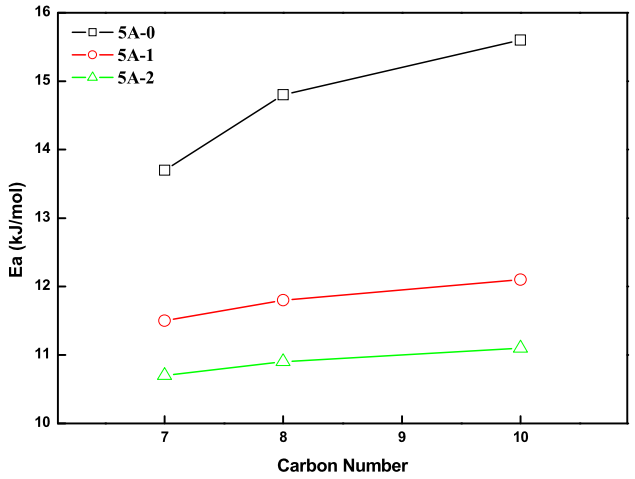

Fig. 8 Change of the activation energy E_a on different 5A zeolites against carbon number

in 5A samples with different mesoporosity follow the order of 5A-2 < 5A-1 < 5A-0, which is in an opposite trend from to the effective diffusion time constants (D_{eff}/R^2). As shown in Table 1 and Fig. 7, there is a significant decrease in activation energy for linear alkanes (e.g. from 14.8 kJ/mol to 10.8 kJ/mol for *n*-octane) with the increase of the mesopore volume. This suggests that the mesopores in the zeolites facilitated the transport of reaction molecules and decreased the adsorption energy barrier due to shorter average diffusion path length and less steric resistance. Figure 8 shows that the activation energy of diffusion increases significantly with carbon number (C_7–C_{10}) in microporous zeolite 5A. This result is in good agreement with the earlier ZLC results by Gunadi and Brandani (2006). However, for the mesoporous zeolites 5A, the activation energy is nearly independent of the carbon number. These results reveal that more pore mouths and shorter diffusion length in the mesoporous structure 5A zeolites significantly decrease the adsorption energy barrier, thus facilitate the transport of reaction molecules.

4 Conclusions

A study of desorption kinetics of *n*-alkanes (C_7–C_{10}) in the mesoporous 5A zeolites was performed using the ZLC method. The effective diffusion time constant (D_{eff}/R^2) obtained from the mesoporous 5A zeolites was higher than that from the microporous zeolite 5A at the same temperature. Effective activation energies on the mesoporous zeolite 5A samples were lower than those on the microporous 5A sample. Compared to the microporous zeolite 5A, the effective activation energy only changed slightly with the carbon number in the mesoporous 5A zeolites. These results suggest that the very short diffusion length and probable intracrystalline mesoporosity in the 5A zeolite samples facilitate kinetics of the molecules through the pores.

Acknowledgements This work was supported by "The National Nature Science Foundation of China" (Grant no. 50872087) and "Research Fund for the Doctoral Program of Higher Education of China" (No. 20111402110005).

References

Cavalcante, C.L., Silva, N.M., Souza-Aguia, E.F., Sobrinho, E.V.: Diffusion of paraffins in dealuminated Y mesoporous molecular sieve. Adsorption **9**, 205–212 (2003)

Eic, M., Ruthven, D.M.: A new experimental technique for measurement of intracrystalline diffusivity. Zeolites **8**, 40–45 (1988a)

Eic, M., Ruthven, D.M.: Diffusion of linear paraffins and cyclohexane in NaX and 5A zeolite crystals. Zeolites **8**, 472–479 (1988b)

Gobin, O.C., Huang, Q.L., Thang, H.V., Kleitz, F., Eic, M., Kaliaguine, S.: Mesostructured silica SBA-16 with tailored intrawall porosity part 2: diffusion. J. Phys. Chem. C **111**, 3059–3065 (2007)

Groen, J.C., Zhu, W.D., Brouwer, S., Huynink, S.J., Kapteijn, F., Moulijn, J.A., Javier, P.R.: Direct demonstration of enhanced diffusion in mesoporous ZSM-5 zeolite obtained via controlled desilication. J. Am. Chem. Soc. **129**, 355–360 (2006)

Gunadi, A., Brandani, S.: Diffusion of linear paraffins in NaCaA studied by the ZLC method. Microporous Mesoporous Mater. **90**, 278–283 (2006)

Hoang, V.T., Huang, Q.L., Malekian, A., Eic, M., Do, T.O., Kalianuine, S.: Diffusion characterization of a novel mesoporous zeolitic material. Adsorption **11**, 421–426 (2005)

Huang, Q.L., Thang, H.V., Malekian, A., Eic, M., Trong-On, D., Kaliaguine, S.: Adsorption of *n*-heptane, toluene and *o*-xylene on mesoporous UL-ZSM5 materials. Microporous Mesoporous Mater. **87**, 224–234 (2006)

Hufton, J.R., Ruthven, D.M.: Diffusion of light alkanes in silicalite studied by the zero length column method. Ind. Eng. Chem. Res. **32**, 2379–2386 (1993)

Jiang, M., Eic, M., Miachon, S., Dalmon, J.A., Kocirik, M.: Diffusion of *n*-butane, isobutane and ethane in a MFI-zeolite membrane investigated by gas permeation and ZLC measurements. Sep. Purif. Technol. **25**, 287–295 (2001)

Lima, P.M., Gonçalves, C.V., Cavalcante, C.L. Jr, Cardoso, D.: Sorption kinetics of linear paraffins in zeolite BEA nanocrystals. Microporous Mesoporous Mater. **116**, 352–357 (2008)

Newalkar, B.L., Choudary, N.V., Kumar, P., Komarneni, S., Bhat, T.S.G.: Exploring the potential of mesoporous dilica, SBA-15, as an adsorbent for light hydrocarbon separation. Chem. Mater. **14**, 304–309 (2001)

Newalkar, B.L., Choudary, N.V., Turaga, U.T., Vijayalakshmi, R.P., Kumar, P., Komarneni, S., Bhat, T.S.G.: Potential adsorbent for light hydrocarbon separation: role of SBA-15 framework porosity. Chem. Mater. **15**, 1474–1479 (2003)

Qiao, S.Z., Bhatia, S.K.: Diffusion of n-decane in mesoporous MCM-41 silicas. Microporous Mesoporous Mater. **86**, 112–123 (2005)

Stefano, B.: Analytical solution for ZLC desorption curves with bi-porous adsorbent particles. Chem. Eng. Sci. **51**, 3283–3288 (1996)

Thang, H.V., Malekian, A., Eic, M., Trong-On, D., Kaliaguine, S.: Diffusive characterization of large pore mesoporous materials with semi-crystalline zeolitic framework. Nanotechnol. Mesostruct. Mater., Proc. 3 Int. Mater. Symp. **146**, 145–148 (2003)

Xue, Z., Ma, J., Hao, W., Ba, X., Kang, Y., Liu, J., Li, R.: Synthesis and characterization of ordered mesoporous zeolite LTA with highion exchange ability. J. Mater. Chem. **22**, 2532–2538 (2012)

Zhao, L., Shen, B.J., Gao, J.S., Xu, C.M.: Investigation on the mechanism of diffusion in mesopore structured ZSM-5 and improved heavy oil conversion. J. Catal. **258**, 228–234 (2008)

Zheng, J.J., Zeng, Q.H., Zhang, Y.Y., Wang, Y., Ma, J.H., Zhang, X.W., Sun, W.F., Li, R.F.: Hierarchical porous zeolite composite with a core–shell structure fabricated using β-zeolite crystals as nutrients as well as cores. Chem. Mater. **22**, 6065–6074 (2010)